Tests of constituent-quark generation methods which maintain both the nucleon center of mass and the desired radial distribution in Monte Carlo Glauber models

J. T. Mitchell, D. V. Perepelitsa, M. J. Tannenbaum, and P. W. Stankus

Tests of constituent-quark generation methods which maintain both the nucleon center of mass and the desired radial distribution in Monte Carlo Glauber models.

J. T. Mitchell, D. V. Perepelitsa, M. J. Tannenbaum

Brookhaven National Laboratory, Upton, NY 11973 USA

P.W. Stankus

Oak Ridge National Laboratory
Oak Ridge TN 37831 USA

Several methods of generating three constituent-quarks in a nucleon are evaluated which explicitly maintain the nucleon's center of mass and desired radial distribution and can be used within Monte Carlo Glauber frameworks. The geometric models provided by each method are used to generate distributions over the Number of Constituent Quark Participants (N_{qp}) in $p+p$, d+Au and Au+Au collisions. The results are compared with each other and to a previous result of N_{qp} calculations, without this explicit constraint, used in measurements of $\sqrt{s_{NN}}$ =200 GeV $p+p$, d+Au and Au+Au collisions at RHIC.

I. GLAUBER MODELS FOR A+B COLLISIONS

In order to calculate the nuclear geometry, i.e. the number of participating nucleons (and more recently constituent-quark participants) in the collision of two nuclei, the Glauber Monte Carlo approach is widely used [1]. The nucleons in the two nuclei are taken to be frozen in position in their respective nucleus during the collision where it is also assumed that the nucleons travel along straight line trajectories which are not affected by any nucleon-nucleon (N+N) collisions. This enables a high-energy nucleus-nucleus (A+B) collision to be simulated in two steps:

(i) Each beam and target nucleus, composed of A and B nucleons respectively is generated by placing the nucleons at random about the position of the nucleus, uniform in $\cos\theta$, ϕ and $r^2 \times \rho_N(r)$ for spherical nuclei, where the nuclear density, $\rho_N(r)$, is typically taken as a Fermi (Woods-Saxon) density function [2]:

$$\frac{d^3\mathcal{P}}{d^3r} = \frac{d^3\mathcal{P}}{r^2 dr \sin\theta d\theta\, d\phi} = \rho_N(r) = \frac{\rho_0}{1 + \exp(\frac{r-c}{a_0})} \quad (1)$$

with $c = \{1.18A^{1/3} - 0.48\}$ fm and the diffusivity $a_0 = 0.545$ fm for Au.

(ii) The coordinates of the two nuclei are then shifted at random relative to each other in a plane transverse to the beam axis by a vector $\vec{b}$, the impact parameter, sampling an area much larger than the range of possible impact parameters for the A+B collision. A pair of nucleons, one from each nucleus, interact with each other if their projected distance d in the plane transverse to the beam axis satisfies the condition:

$$d \leq \sqrt{\frac{\sigma_{N+N}^{\mathrm{inel}}}{\pi}} \quad (2)$$

where $\sigma_{N+N}^{\mathrm{inel}}$ is the inelastic nucleon-nucleon cross section.

The nuclear geometrical parameters such as N_{part}, the number of participating nucleons, N_{coll}, the number of binary $N + N$ collisions, etc., can be computed for each trial.

A. Constituent Quarks

The approach can be extended one level further down with an additional step:

(iii) modeling each nucleon by generating the positions of the three constituent-quarks (q) within it [3–5], effectively creating a constituent-quark structure of each nucleus. The A+B collision represented as a sum of $q+q$ collisions is then obtained by changing the word "nucleon" to "quark" and $N + N$ to $q + q$ in step (ii) above.

II. E_T AND N_{CH} DISTRIBUTIONS AND EXTREME INDEPENDENT MODELS (EIM)

Measurements of mid-rapidity transverse energy distributions $d\mathrm{E}_T/d\eta$ in $p+p$, d+Au and Au+Au collisions at $\sqrt{s_{NN}}$ =200 GeV were recently presented by the PHENIX collaboration [6]. The transverse energy E_T, a multiparticle variable dominated by soft particles and closely related to the multiplicity of charged particles N_{ch} [7], is defined as the sum

$$\mathrm{E}_T = \sum_i E_i \sin\theta_i$$

$$d\mathrm{E}_T(\eta)/d\eta = \sin\theta(\eta)\, dE(\eta)/d\eta \quad , \quad (3)$$

where θ is the polar angle, $\eta = -\ln\tan\theta/2$ is the pseudorapidity, E_i is by convention taken as the kinetic energy

for baryons, the kinetic energy $+ 2 m_N$ for antibaryons, and the total energy for all other particles, and the sum is taken over all particles emitted into a fixed solid angle for each event. The PHENIX measurement [6] showed that the number of constituent-quark participants N_{qp} represented the fundamental elements of particle production at mid-rapidity in all 3 systems.

The data were analyzed in the Extreme Independent Model (EIM) framework in which the effect of the nuclear geometry of the interaction can be calculated independently of the dynamics of particle production, which can be derived from experimental measurements, usually the $p+p$ (or $p+A$) measurement in the same detector. The nuclear geometry of the collisions is usually calculated in a Glauber Monte Carlo Calculation [1] and represented as the relative probability of the number n of fundamental elements of particle production, called weights w_n, with $n = 1$ or 2 as a minimum, to a maximum value N_{max}. EIMs, which have been popular since the first measurements of particle production in relativistic $p+A$ and A+A collisions successfully describe N_{ch} and E_T distributions in different ranges of c.m. energies $\sqrt{s_{NN}}$. A representative sample includes the wounded-nucleon (or nucleon-participant N_{part}) model (WNM) [8], wounded-projectile-nucleon Model (WPNM) [9–11], additive-quark-model (AQM) [12] which is equivalent to a wounded-projectile-quark (color-string) model, constituent-quark-participant model (NQP) [6] and quark-diquark model [13] (where the names reflect the fundamental element of particle production, nucleons or constituent-quarks. [1])

At RHIC ($\sqrt{s_{NN}} = 19.6 - 200$ GeV), PHOBOS [14] has shown that the WNM works in Au+Au collisions for the total multiplicity, N_{ch}, over the range $|\eta| < 5.4$, while at mid-rapidity, the WNM fails—the multiplicity density per participant pair, $\langle dN_{ch}/d\eta \rangle /(N_{part}/2)$, increases with increasing number of participants, in agreement with previous PHENIX results [7, 15, 16]. Additionally, it was shown using PHOBOS Au+Au data [17, 18] and discussed for other data [19] that the mid-rapidity $\langle dN_{ch}/d\eta \rangle$ as a function of centrality in Au+Au collisions is linearly proportional to the number of constituent-quark participants (NQP); however for symmetric systems this cannot be distinguished from the number of color-strings, the AQM [20].

PHENIX [6] then demonstrated, using mid-rapidity E_T distributions at $\sqrt{s_{NN}} =200$ GeV in the asym-

metric d+Au system, as well as $p+p$ and Au+Au collisions, that the asymmetric d+Au measurement, which is crucial in distinguishing the color-string (AQM) from NQP models, clearly rejects the AQM and agrees very well with the NQP model. The NQP model also explained that the two-component ansatz, $dE_T/d\eta \propto (1-x)N_{part}/2 + xN_{coll}$, which has been used to describe E_T and charged-multiplicity (N_{ch}) distributions as a function of centrality, works because the particular linear combination of N_{part} and N_{coll} is an empirical proxy for N_{qp} and not because the N_{coll} implies a hard-scattering component in E_T or N_{ch} distributions (which is known to be absent in $p + p$ collisions [21, 22]).

A. Previous methods of generating the positions of the constituent-quarks

The first 3 calculations which showed that N_{ch} was linearly proportional to N_{qp} [17–19] only studied Au+Au collisions and simply generated three times the number of nucleons according to the Au radial disribution, Eq. 1, called them constituent-quarks and let them interact with the conventional constituent $q + q$ cross section $\sigma_{q+q}^{inel} = \sigma_{N+N}^{inel}/9$, e.g $\sigma_{q+q}^{inel}=41\text{mb}/9=4.56$ mb at $\sqrt{s_{NN}}$ $=130$ GeV [17].

The PHENIX2014 method [6] was different from these N_{qp} calculations in that it used the E_T distribution measured in $p + p$ collisions to derive the E_T distribution of a constituent-quark to use as the basis of the calculations of the d+Au and Au+Au distributions. In PHENIX2014 [6], the spatial positions of the three quarks were generated around the position of each nucleon in the Glauber Monte Carlo calculations for $p + p$, d+Au and Au+Au collisions using the proton charge distribution corresponding to the Fourier transform of the form factor of the proton [2, 23]:

$$\rho^{proton}(r) = \rho_0^{proton} \times \exp(-ar), \qquad (4)$$

where $a = \sqrt{12}/r_m = 4.27$ fm^{-1} and $r_m = 0.81$ fm is the r.m.s radius of the proton weighted according to charge [2]

$$r_m = \int_0^\infty r^2 \times 4\pi r^2 \rho^{proton}(r)dr \qquad . \qquad (5)$$

The corresponding proton form factor is the Hofstadter dipole fit [24] now known as the standard dipole [25]:

$$G_E(Q^2) = G_M(Q^2)/\mu = \frac{1}{(1 + \frac{Q^2}{0.71\text{GeV}^2})^2} \qquad (6)$$

where G_E and G_M are the electric and magnetic form factors of the proton, μ is its magnetic moment and Q^2 is the four-momentum-transfer-squared of the scattering. The inelastic $q + q$ cross section $\sigma_{q+q}^{inel} = 9.36\text{mb}$ at $\sqrt{s_{NN}}$ $=200$ GeV was derived from the $p + p$ N_{qp} Glauber calculation by requiring the calculated $p + p$ inelastic cross

---

[1] In the AQM, unlike the other models, a distinction is made between the number of constituent-quark participants and the mechanism of particle production which is by color strings between the quark participants with the restriction of only one color string attached to a quark-participant. In an asymmetric A+B collision, this restriction limits the number of color-strings to the number of constituent-quarks in the smaller nucleus so is effectively a projectile-quark-participant model, while the NQP model allows all the quark-participants in both nuclei to emit particles.

section to reproduce the measured $\sigma_{N+N}^{\text{inel}} = 42$ mb cross section, and then used for the d+Au and Au+Au calculations (Fig. 1) [6].
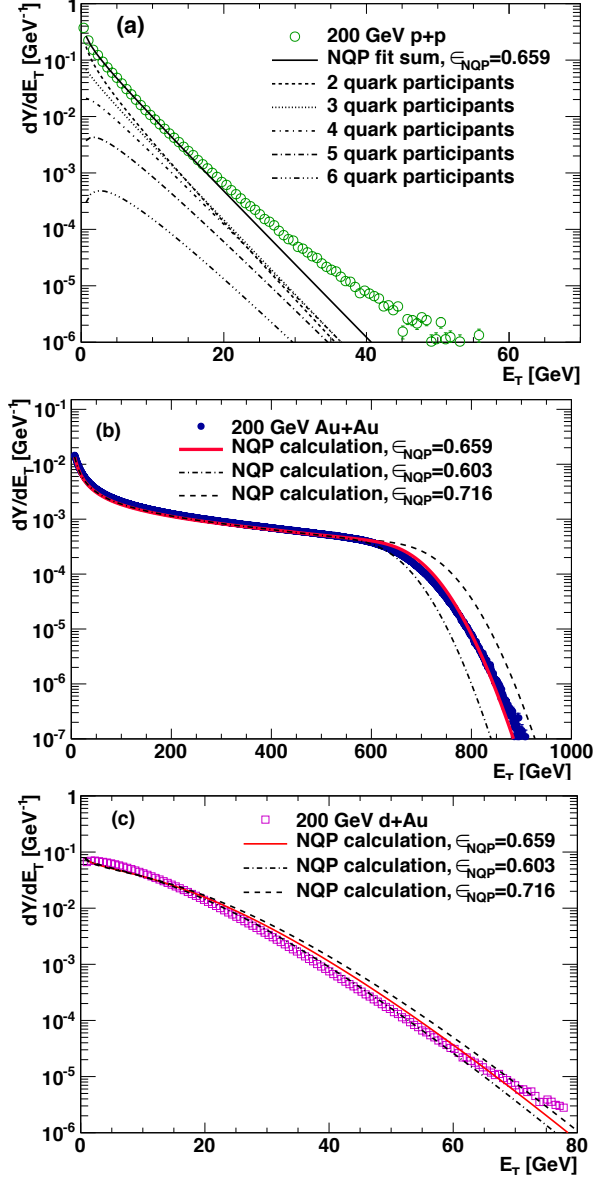

FIG. 1. PHENIX2014 [6] method for $\mathrm{E}_T \equiv d\mathrm{E}_T/d\eta|_{y=0}$ distributions at $\sqrt{s_{NN}} = 200$ GeV: a) Deconvolution fit to the p+p E_T distribution for $\mathrm{E}_T < 13.3$ GeV with the corrected weights w'^{NQP}_i with $\epsilon_{NQP} = 1 - p_{0_{\text{NQP}}} = 0.659$ calculated in the Number of Quark Participants or N_{qp} model. Lines represent the properly weighted individual E_T distributions for the underlying 2,3,4,5,6 constituent-quark participants plus the sum. b) Au+Au compared to the NQP calculations using the central $1 - p_0 = 0.647$ and $\pm 1\sigma$ variations of $1 - p_0 = 0.582, 0.712$ for the probability p_0 of getting zero E_T on a p+p collision with resulting $\varepsilon_{\text{NQP}} = 0.659, 0.603, 0.716$, respectively. c) d+Au calculation for the same conditions as in (b).

Yet another method was used in the quark-diquark calculation [13] where the quark-diquark system for a pro-

ton was generated so that it maintained the same center of mass as the original proton. The radius of the quark $\vec{r}_q$ was generated according to a gaussian with the r.m.s. charge radius of the proton and then the diquark is put at half the radius of the quark and vectorially opposite, $\vec{r}_q + 2\vec{r}_{qq} = 0$. This was not the case for the PHENIX2014 method and is generally not the case for Glauber Monte Carlo calculations in large nuclei. However, it was pointed out [2] that not maintaining the proton c.m. might pose a problem. The generated radii of the three quarks, $\vec{r}_1$, $\vec{r}_2$, and $\vec{r}_3$ follow the correct charge distribution (Eq. 4) about the original proton center, $\vec{r} = 0$; but the origin of the generated quark-triplet proton calculated by the vector sum of the three quark positions, $\vec{r}_p \equiv \vec{r}_1 + \vec{r}_2 + \vec{r}_3$, will not likely sum to zero, the position of the original proton. Thus, the radial distributions of all the generated quark-triplets computed about the position $\vec{r}_p$ in each case would be different than the true proton radial distribution and rms radius (Eq. 4). This latter problem is shared by the quark-diquark method.

To determine the effects, if any, of the issues raised above about the PHENIX2014 [6] method, three new methods of generating constituent-quarks around a nucleon are presented which will keep the origin of each generated quark-triplet the same as the original nucleon and maintain the desired radial charge distribution. The NQP model calculations are then performed using the PHENIX2014 data [6].

III. IMPROVED METHODS OF GENERATING THE POSITIONS OF CONSTITUENT-QUARKS AROUND A NUCLEON

Here we describe our operational methods for generating the positions of constituent-quarks within a nucleon. Without delving into the full information on nucleon internal structures as revealed in deep inelastic scattering, we construct our model of quark positions by simply assuming that their spatial distributions follow the profile of the charge distribution of the proton, relative to the system's center of mass, as measured through elastic electron scattering [2, 23]. Generally, then, to simulate a set of n constituents we need a procedure to produce n random vectors $(\vec{x}_1, ..., \vec{x}_n)$ subject to the conditions

(1) Assuming all the constituents to have the same mass, the sum of their positions $\sum \vec{x}_i$ must be identical for all instantiations of $(\vec{x}_1, ..., \vec{x}_n)$, to respect the fixed, given position of the nucleon center of mass; for simplicity we can require $\sum \vec{x}_i = 0$ for any one nucleon's constituents within its coordinate system;

(2) The distribution of $\vec{x}_i$ for each individual constituent should follow some function $\rho(\vec{x})$ which corre-

———

[2] Thanks to Adam Bzdak and Peter Steinberg for bringing this to our attention.

sponds to the measured charge distribution of the proton around its center of mass.

Elastic scattering measurements on a charge cloud constrain the (charge-averaged) individual spatial distributions of the cloud's constituents around the center of mass; but they do not constrain the correlations among the constituents. Accordingly, we will describe and test here a variety of procedures for generating the n vectors $(\vec{x}_1, ..., \vec{x}_n)$ which satisfy (1) and (2) above but which span a wide range in correlation behavior. In all methods described below we take the masses and electrical charges of the constituents to be equal, for simplicity; and we follow these prescriptions for all methods:

Notation: The magnitude of a position vector is denoted by $r \equiv |\vec{x}|$, and $r_i \equiv |\vec{x}_i|$. The unit vector $\hat{u}$ represents a random direction chosen uniformly over the sphere. For each method we will assume a general number of constituents n; though we will focus on the $n = 3$ case for nucleons in this paper we also investigate the effect of 2,4 and 5 constituent-quarks in the PHENIX2014 [6] method to reflect, for instance, the presence of sea quarks or gluons.

Parent distribution: For the charge distribution satisfied by the generated quark-triplets about their center of mass, the goal is to reproduce Eq. 4.

We note that none of the previous Glauber Monte Carlo calculations cited in Sec. II A satisfied both conditions (1) and (2) above; and we believe that this report is the first to do with comparison to measured E_T distributions in $p + p$, d+Au and Au+Au collisions. As we shall see, these departures from the desired radial distribution (Eq. 4) are vanishing in the limit of large n, but for $n = 3$, as in constituent-quarks in a nucleon, the differences between the present and previous constructions are small but informative [26].

A. Planar Polygon

Generate one quark at $(r, 0, 0)$ with r drawn from $r^2 \rho^{\text{proton}}(r)$. Then instead of generating $\cos\theta$ and ϕ at random and repeating for the two other quarks as was done by PHENIX2014 [6], imagine that this quark lies on a ring of radius r from the origin and place the two other quarks on the ring at angles spaced by $2\pi/3$ radians. Then randomize the orientation of the 3-quark ring spherically symmetric about the origin. This guarantees that the radial density distribution is correct about the origin and the center of mass of the three quarks is at the origin but leaves the three-quark-triplet on each trial forming an equilateral triangle on the plane of the ring which passes through the origin.

An evident problem with this model is that it introduces a correlation because all quarks on a given trial have the same radius from the center of the proton. An advantage of this model is that it can be easily applied

to any number, n, of quarks distributed around the ring of radius r at angles spaced by $2\pi/n$ radians.

B. Explicit Joint distribution

In this method we construct the joint distribution explicitly to satisfy conditions (1) and (2) above, and to be symmetric among the constituents, but otherwise to have minimal correlations between them. With the use of an auxiliary probability distribution function $f(\vec{x})$ we write the joint distribution over all n vectors simply as

$$P(\vec{x}_1, ..., \vec{x}_n) = f(\vec{x}_1) f(\vec{x}_2) ... f(\vec{x}_n) \delta\left(\sum \vec{x}_i / n\right) \quad (7)$$

where the Dirac delta $\delta()$ insures the center-of-mass condition but the constituents are otherwise as independent as possible.

To get an operational procedure from this definition we need to specify two things: (I) how to chose the auxiliary distribution $f(\vec{x})$ such that the singles distribution of each $\vec{x}_i$ follows $\rho(\vec{x})$; and (II) given an $f(\vec{x})$, how do we chose a set $(\vec{x}_1, ..., \vec{x}_n)$ which will follow the joint distribution in Eq. 7. We answer these as follows.

(I) Let $f^{[k]}(\vec{x})$ be defined as the kth-order 3-D convolution of $f(\vec{x})$ with itself; e.g. $f^{[2]}(\vec{x}) = f(\vec{x}) \circ \circ \circ f(\vec{x})$. Then it can be shown from Eq. 7 that for the singles distribution of any individual $\vec{x}_i$ to follow $\rho(\vec{x})$ the auxiliary function $f()$ must satisfy

$$\rho(\vec{x}) = f(\vec{x}) f^{[n-1]}(-\vec{x}) \quad . \quad (8)$$

In practice it may not be straightforward to invert Eq. 8 and determine $f()$ given $\rho()$; instead it may be sufficient to use an auxiliary $f(\vec{x})$ determined by trial and error to match the desired $\rho(\vec{x})$. For this paper the implementation is with such a trial and error determination; the auxiliary function defined with two parameters b and c

$$f(\vec{x}) = \exp{-(b\,r/r_0)} \left[1 + \left(\frac{r}{c\,r_0}\right)\right] \quad (9)$$

with $c = 3.9$ and $b = 0.91$ and $r_0 = r_m/\sqrt{12}$ will result in a singles distribution that matches the Hofstadter profile [23] Eq. 4 to within a few percent out to $r < 10r_0 = 2.3\text{fm}$.

(II) Once the auxiliary function $f()$ is chosen, how do we operationally generate random sets of position vectors $(\vec{x}_1, ..., \vec{x}_n)$, distributed according to the probability density in Eq. 7. One simple, all-purpose approach to generating random variables according to any given distribution is *rejection sampling.*

In its simplest form, one can calculate the center of mass of the generated vectors, $x_{CM} = \Sigma \vec{x}_i / n$ and keep the sample if and only if x_{CM} is within some tolerance

limit of zero, to enforce the effect of the delta function $\delta(\Sigma \vec{x}_i/n)$. This method is numerically inefficient as only a small fraction of generated sets will be kept; and becomes less efficient the stricter the tolerance for $x_{CM} \to 0$.

Fortunately, we can use rejection sampling in a much more numerically efficient algorithm, which will keep on the order of $1/5$–$1/10$ of the initially generated selections and without degrading with increasing n, vis:

(1) Generate all but one of the vectors $\vec{x}_i$ independently, each according to $f(\vec{x})$; which one of the list is not chosen here is unimportant, let's suppose it is $\vec{x}_1$; then

(2) Calculate the value of the remaining vector as the negative sum of all the previously chosen ones, e.g. $\vec{x}_1 = -(\vec{x}_2 + ... + \vec{x}_n)$ to enforce the center of mass at zero; then

(3) Keep this sample if and only if a new random number chosen uniformly on $[0, 1]$ is less than or equal to the probability density of the final vector, $f(\vec{x}_1)$; otherwise reject the sample and try again.

C. Recentered approach with empirical radial distribution

In this method, the three constituent-quark positions are drawn independently from an auxiliary function $f(r)$, and then the center of mass of the generated three-quark system is re-centered to the original nucleon position. The empirical function, $f(r)$ (Eq. 10), is chosen such that the resulting radial quark distribution $\rho(r)$ with respect to the center of mass (i.e. after re-centering) reproduces the proton charge distribution, $\rho^{\text{proton}}(r)$ (Eq. 4), the Fourier transform of the proton form factor, as measured in electron-proton elastic scattering [23] (Fig. 2). For the results presented here, this function was chosen to be[3]

$$f(r) = r^2 \rho^{\text{proton}}(r)(1.21466 - 1.888r + 2.03r^2) \\ (1 + 1.0/r - 0.03/r^2)(1 + 0.15r) \quad (10)$$

where r is the radial position of the quark in fm. The polar and azimuthal positions of each quark are generated uniformly in $\cos\theta$ and ϕ to achieve a spherically symmetric distribution. Once all of the quark coordinates are determined, the three quark system is shifted so that the center of mass matches the center position of the nucleon.

This function was derived through an iterative, empirical approach. For a given test function $f^{\text{test}}(r)$, the resulting radial distribution $\rho^{\text{test}}(r)$ was compared to the desired distribution $\rho^{\text{proton}}(r)$ in Eq. 4. The ratio of $\rho^{\text{test}}(r)/\rho^{\text{proton}}(r)$ was parameterized with a polynomial

---

[3] This function was derived by D. V. Perepelitsa and used in Ref. [26].

function of r or $1/r$, and the test function was updated by multiplying it with this parametrization of the ratio. Then, the procedure was repeated until the ratio $\rho^{\text{test}}(r)/\rho^{\text{proton}}(r)$ was sufficiently close to unity over a wide range of r values. The resulting functional form for $f(r)$ is given above in Eq. 10. A future determination of $f(r)$ may yield an incrementally better agreement between the resulting $\rho(r)$ and the desired Hofstadter standard-dipole form, $\rho^{\text{proton}}(r)$ (Eq. 4), but we believe the present form is close enough for our practical purposes.

This method is conceptually the most similar to the previous PHENIX2014 [6] method of generating constituent-quark systems, which was described in Section II A. That method effectively followed the approach defined here but used an auxiliary function equal to the desired proton charge distribution, $f(r) = \rho^{\text{proton}}(r)$ (Eq. 4). Thus, the resulting $\rho(r)$ with respect to the center of mass (i.e. after re-centering) in the PHENIX2014 [6] method was different from $\rho^{\text{proton}}(r)$ (Fig. 3).
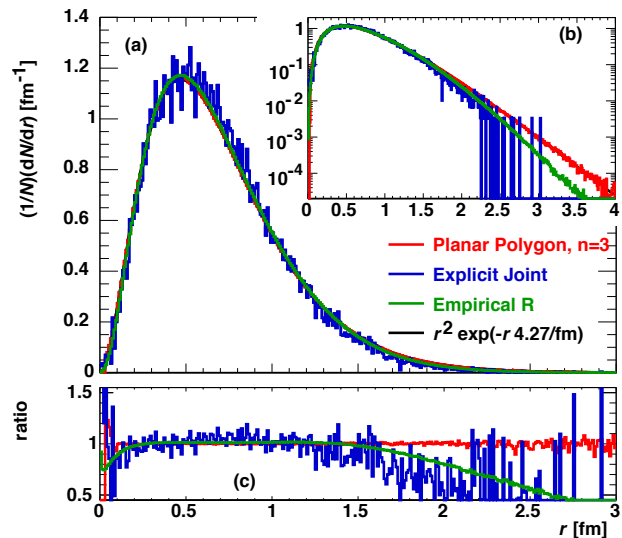

FIG. 2. a) Radial distribution $d\mathcal{P}/dr$ about the c.m. of the generated quark-triplets as a function of r [fm] for the three methods: (red) Planar Polygon (Sec. III A); (blue) Explicit Joint (Sec. III B); (green) Empirical Recentered (Sec. III C); compared to $r^2\rho^{\text{proton}}(r)$ from Eq. 4 (black), with a semi-log plot shown as the inset (b). (c) Ratio of the generated distributions to Eq. 4. The Planar Polygon distribution is identical to $r^2\rho^{\text{proton}}(r)$ so obscures the black line.

D. Comparison of the three new methods

Fig. 2 shows the resulting radial distributions in each of the three new methods compared to $r^2\rho^{\text{proton}}(r)$ from Eq. 4. The Planar Polygon (Sec. III A) radial distribution $d\mathcal{P}/dr$ about the c.m. of the generated quark-triplet is identical to the input proton charge distribution Eq. 4
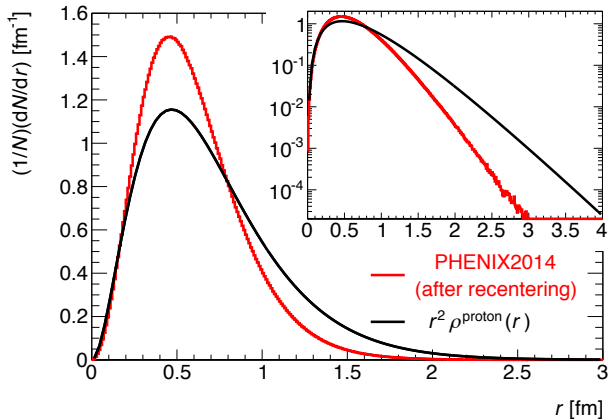
FIG. 3. Radial distribution $d\mathcal{P}/dr$ about the c.m. of the generated quark-triplets as a function of r [fm] for the PHENIX2014 [6] method compared to $r^2\rho^{\mathrm{proton}}(r)$ from Eq. 4.

by construction. However, it has the problem that all 3 quarks in each proton have the same radius from the center and lie in a plane, which passes through the c.m., on the points of an equilateral triangle—an unlikely correlation in nature. The Explicit Joint distribution method (Sec. III B) follows Eq. 4 to $r \approx 1.5$ fm, almost as well as noted in Sec. III B, but has issues at small r and is relatively inefficient to generate as shown by the large statistical fluctuations. The Empirical Recentered approach (Sec. III C) follows Eq. 4 to $r \approx 2$ fm, is straightforward to generate and is spherically symmetric, so is likely the best of the three new methods. We further note that unlike the Explicit Joint distribution method (Sec. III B), each application of this method results in a usable three-quark configuration, making it the more computationally efficient of the two.

We are now in a position to apply these three methods to Monte Carlo Glauber Model calculations of $p + p$, d+Au and Au+Au measurements with constituent-quarks as the fundamental elements of particle production, the NQP model.

E. Sensitivity to the number of constituent-quarks per proton

Although the massive constituent-quarks which form mesons and baryons (e.g. a proton=uud) are relevant for the static properties of hadrons[3–5] and soft hadron physics such as $dN_{\mathrm{ch}}/d\eta$ and $dE_T/d\eta$, predominantly composed of particles with $p_T \lesssim 1.4$ GeV/c where the p_T distributions of p, K and π are exponential [27], there is often a confusion with massless partons (gluons and current quarks) which are typically only evident in hard scattering with $p_T \gtrsim 3$ GeV/c where the p_T distributions follow a power-law. Thus, the question typically arises as to whether the NQP model works for an arbitrary number of quarks. We have investigated this for the $dN_{\mathrm{ch}}/d\eta$ measurements of Ref. [26] using the PHENIX2014 method [6] of constituent-quark generation which can easily be ap-

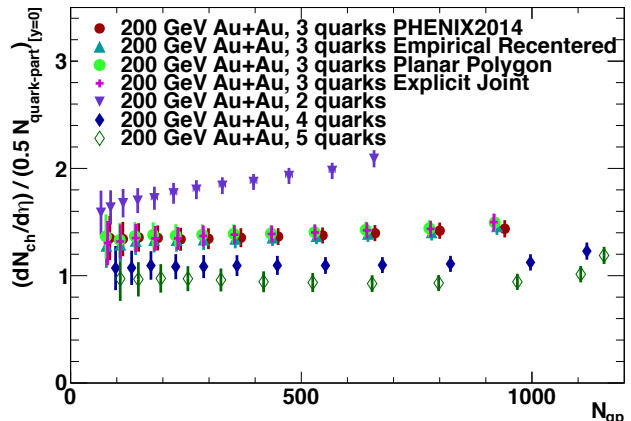plied to 2,3,4,5 constituent-quarks, and compared the results to the present methods for 3 consituent-quarks. The

FIG. 4. $dN_{\mathrm{ch}}/d\eta/(0.5N_{\mathrm{qp}})$ at mid-rapidity as a function of N_{qp} for $dN_{\mathrm{ch}}/d\eta$ measurements [26] in Au+Au collisions at $\sqrt{s_{NN}}$ =200 GeV. The various methods and number of constituent-quarks assumed per proton are given in the legend.

results for $dN_{\mathrm{ch}}/d\eta/(0.5N_{\mathrm{qp}})$ in Au+Au at $\sqrt{s_{NN}}$ =200 GeV, shown in Fig. 4, indicate that 2 constituent-quarks are rejected while 3 constituent-quarks give essentially the same result for all 4 methods, and 4 or 5 constituent-quarks seem to work as well as 3 in this calculation.

It is also noteworthy that the difference between $dN_{\mathrm{ch}}/d\eta/(0.5N_{\mathrm{qp}})$ in PHENIX2014 [6] and the present Empirical Recentered approach (Sec. III C) is $\lesssim 2\%$.

IV. COMPARISON OF THE NEW METHODS TO PHENIX2014 RESULTS

The results for NQP calculations for measurements of E$_T$ distributions in $p + p$, d+Au and Au+Au collisions at $\sqrt{s_{NN}}$ =200 GeV with the PHENIX2014 constituent-quark generation method [6] have been shown in Fig. 1. The conclusions were that starting with the E$_T$ distribution of a constituent-quark derived by deconvoluting the $p + p$ E$_T$ distribution according to the number of constituent-quark participants in a $p + p$ collision, both the shape and magnitude of the E$_T$ distributions in d+Au and Au+Au calculated in the NQP model are in excellent agreement with the measurements. The NQP calculations will now be repeated here using the new methods that keep the origin of each generated quark-triplet the same as the original proton and preserve the generated proton charge distribution. However, because the calculations are quite detailed, they will be fully described in an appendix, following the presentation of the results and conclusions.

A. NQP Calculations of the $p+p$ distributions

Calculations of the $q+q$ cross sections σ_{q+q} and relative probabilities w_n for $n = 2,3,4,5,6$ constituent-quark participants in $p+p$ collisions, for the PHENIX2014 and the three new methods are given in Table I. These are derived from Glauber Monte Carlo calculations in each method which vary σ_{q+q} until the calculated value for the inelastic cross section in $p+p$ collisions is 42 mb (for $\sqrt{s_{NN}}$ =200 GeV) [6]. This is purely nuclear geometry.

A correction to the weights is then applied to account for the fact that only a fraction ϵ_{p+p} of $p+p$ collisions produces non-zero E_T in the detector. Gamma distribution parameters p and b of 1 constituent-quark-participant are then derived in each method from deconvolution fits to measured $p + p$ E_T distribution and applied to calculations of E_T distributions in the various collision systems.

The calculations of the $p+p$ E_T distribution are shown in Fig. 5a for the Empirical Recentered method and in Figs. 9a, 10a for the Planar Polygon and Explicit Joint methods, respectively, using the Gamma distribution parameters p and b for the E_T distribution of 1 constituent-quark-participant derived from the deconvolution fits to the same data (Table V). The deconvolution fits and and the NQP calculations of the $p + p$ E_T distribution using the derived b and p parameters are separate calculations, so the excellent agreement of the $p+p$ data with the calculations shows that the three new methods work as well as the PHENIX2014 method [6] (Fig. 1a).

B. NQP Calculations of the Au+Au distributions

The Au+Au calculations are shown in Fig. 6 with details in Fig. 5b and Figs. 9b, 10b which may be compared to Fig. 1b. The Planar Polygon and Empirical Recentered methods agree quite well with the PHENIX2014 [6] calculation and the data but they show 10% and 7% more E_T respectively. The surprising result is that the most sophisticated but computing intensive Explicit Joint method comes out virtually on top of the simplest Planar Polygon method rather than in agreement with the Empirical Recentered method.

More important to note is that the agreement of the new centered methods with the Au+Au data is within the 1σ uncertainty of the Empirical Recentered calculation in Figure 5b (i.e. the curve of -1σ with $\epsilon_{\mathrm{NQP}} = 0.636$ lies essentially on top of the data) and within 1.5σ of the Planar Polygon calculation in Figure 9b. Also, the new calculations agree with PHENIX 2014 calculation [6] (Fig. 6) to within 1.2σ of its uncertainty for the Empirical Recentered method and 1.8σ for the Planar Polygon method.

C. d+Au and AQM vs NQP

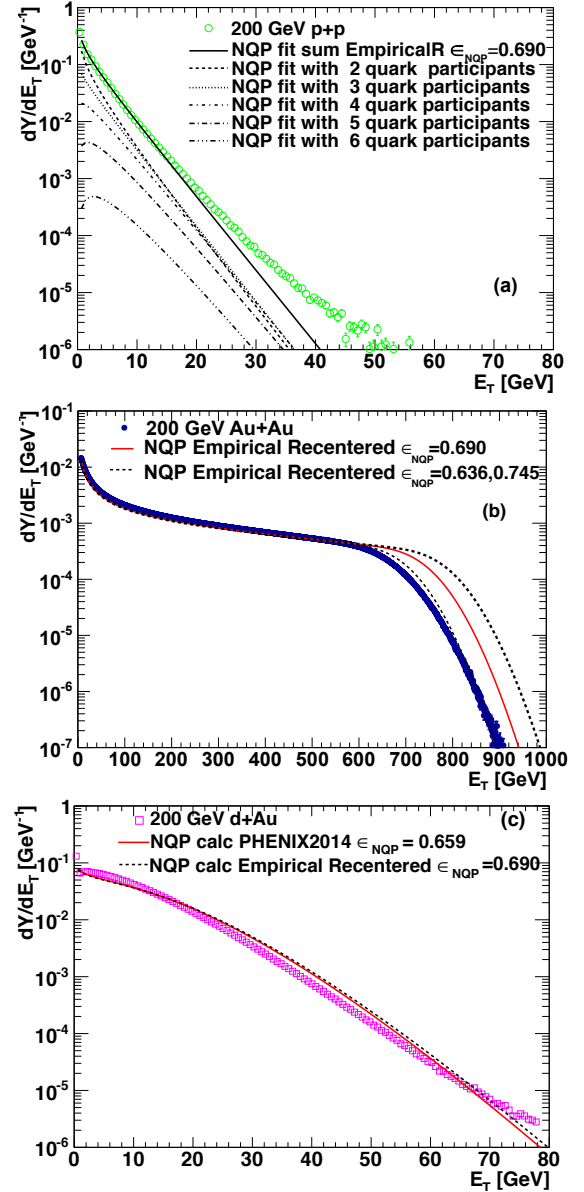One of the principal issues of PHENIX2014 [6] was that an asymmetric system such as d+Au was required

FIG. 5. $\mathrm{E}_T \equiv d\mathrm{E}_T/d\eta|_{y=0}$ distributions at $\sqrt{s_{NN}} = 200$ GeV calculated in the Number of Quark Participants (NQP) model from the Empirical Recentered (Sec. III C) method with $\epsilon_{NQP} = 1 - p_{0_{NQP}} = 0.690$. a) NQP calculation of the $p+p$ E_T distribution for $\mathrm{E}_T < 13.3$ GeV with the parameters p and b for the E_T distribution of 1 QP from the deconvolution fit to the same data (Table V) where the thin lines shown are the E_T distributions for 2,3,4,5 and 6 QP weighted by w'_n from Table III and the thick line is the sum. b) Au+Au compared to the NQP calculations using the central $1-p_0 = 0.647$ and $\pm1\sigma$ variations of $1-p_0 = 0.582, 0.712$ for the probability p_0 of getting zero E_T on a $p+p$ collision [6] with resulting $\varepsilon_{\mathrm{NQP}} = 0.690, 0.636, 0.745$, respectively. c) d+Au calculation for the same conditions as in (b) and for PHENIX2014 [6].

to resolve the difference between the Additive Quark Model—a color string model with the restriction of one color string per constituent-quark participant, or a maximum of 6 strings in d+Au compared to 3 in $p+p$—and the constituent-quark model which counts all the struck
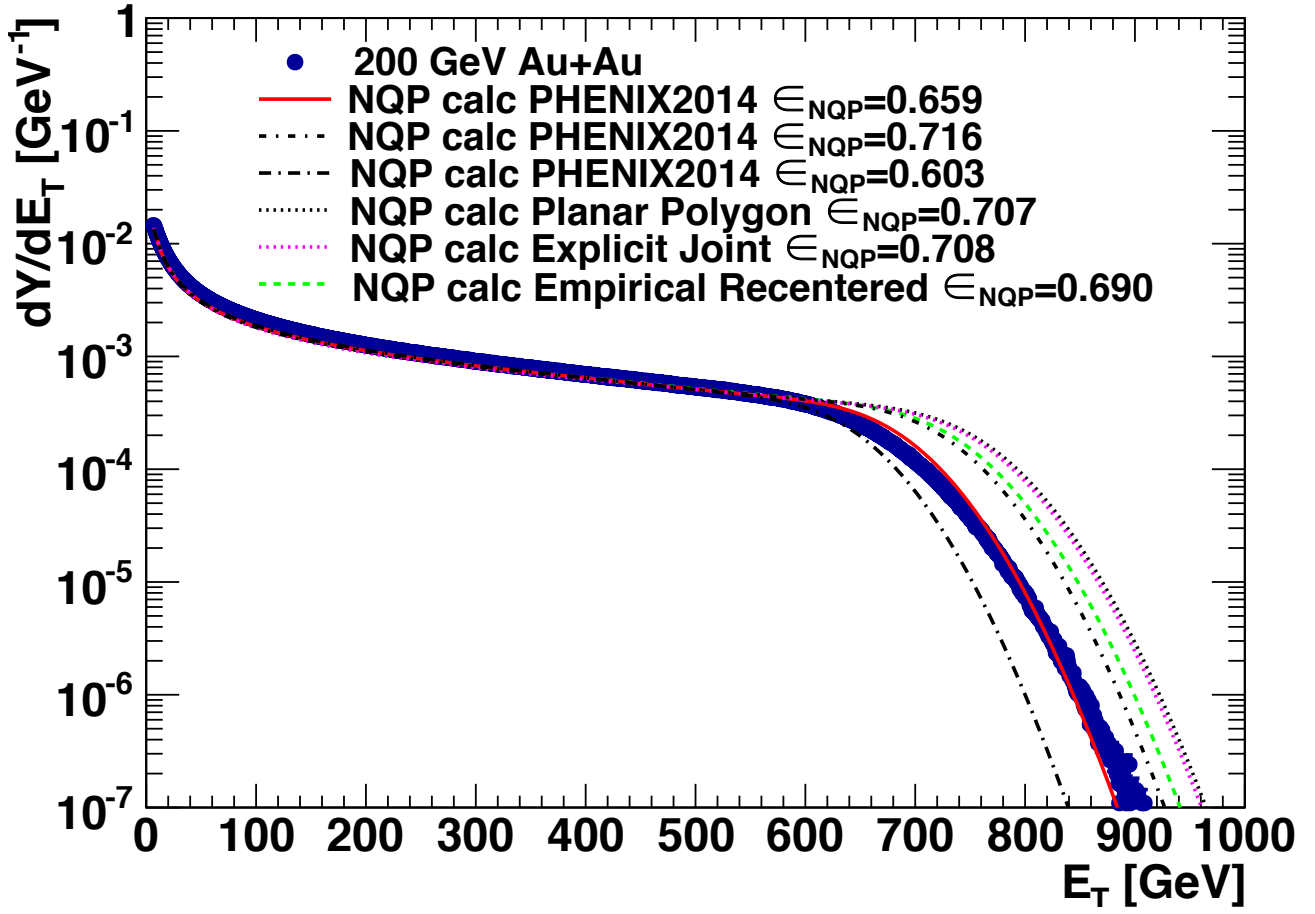
FIG. 6. PHENIX2014 [6] E$_T$ distribution in Au+Au at $\sqrt{s_{NN}} = 200$ GeV compared to the Number of Quark Participants (NQP) model calculations indicated, where ϵ_{NQP} represents the probability for a constituent quark participant to give non-zero E$_T$ in the detector. The PHENIX2014 NQP calculation is shown for the central value, $\epsilon_{NQP} = 0.659$, and the $\pm 1\sigma$ systematic variations in $\epsilon_{NQP} = 0.716, 0.603$ [6] as detailed in Fig. 1.

quarks in the Au target for producing particles. The result [6] was that the AQM indicated a factor of 1.7 less E_T than the NQP, while the NQP is in excellent agreement with the data. The good news is that a calculation of the NQP model for d+Au with the Empirical Recentered method gives a result which is essentially indistinguishable from the PHENIX2014 [6] NQP result and the data (Fig. 5c).

D. Status of the two-component ansatz as an empirical proxy for N_{qp}

It has been popular since PHENIX [15], inspired by the previous article in the same journal [28], fit their measurement of the multiplicity distribution in Au+Au collisions at $\sqrt{s_{NN}}$ =130 GeV to the equation:

$$dN_{ch}{}^{AA}/d\eta = dN_{ch}{}^{pp}/d\eta \left[(1-x)\langle N_{part}\rangle/2 + x\langle N_{coll}\rangle\right] \quad (11)$$

with $x \approx 0.16 \pm 0.06$. PHOBOS [29] also found that their measurement of $dN_{ch}{}^{AA}/d\eta$ in Au+Au at $\sqrt{s_{NN}}$ =200 GeV was consistent with Eq 11 with $x = 0.09$ and also noted that their data were consistent with a constant value of $x \approx 0.13 \pm 0.05$ from $\sqrt{s}$ =19.6 to 200 GeV, more recently extended to $x \approx 0.10 - 0.12$ from $\sqrt{s_{NN}}$ =19.6 GeV to $\sqrt{s_{NN}} = 2.76$ TeV (Pb+Pb) [30]. In PHENIX2014 [6] it was shown that the ansatz $[(1-x)\langle N_{part}\rangle/2 + x\langle N_{coll}\rangle]$ in Eq. 11 works because the particular linear combination of N_{part} and N_{coll} turns out to be an empirical proxy for N_{qp} and not because the N_{coll} term implies hard-scattering in N_{ch} and E_T distributions—the ratio of $\langle N_{qp}\rangle$/ansatz with $x = 0.08$ varied by less than 1% over the centrality range 0-80% in 5% bins. Given the new centered methods of calculating the N_{qp}, does this relation still hold?

Figure 7a shows the linearity of N_{qp} vs. the ansatz in the Empirical Recentered method compared to the PHENIX2014 [6] result, with the best values of x in each case; and Fig. 7b the deviations of $\langle N_{qp}\rangle$/ansatz/$\langle\langle N_{qp}\rangle$/ansatz$\rangle$ from 1.00 on an expanded scale (bottom) which are $\lesssim$1.0% for Ref. [6] and $\lesssim$1.5% for the Empirical Recentered method. This shows that the NQP model with either the PHENIX2014 [6] or the Empirical Recentered method are consistent from $p + p$ to Au+Au collisions and so actually work better than the ansatz (which does not extrapolate back to the $p + p$ value [6]).

V. CONCLUSION

The three centered NQP calculations do not deviate from the PHENIX2014 [6] calculation of the $\sqrt{s_{NN}}$ =200 GeV Au+Au E_T distribution by more than $1 - 1.5$ standard deviations of their systematic uncertainties. The surprising result is that the most sophisticated but computing intensive Explicit Joint method comes out virtu-
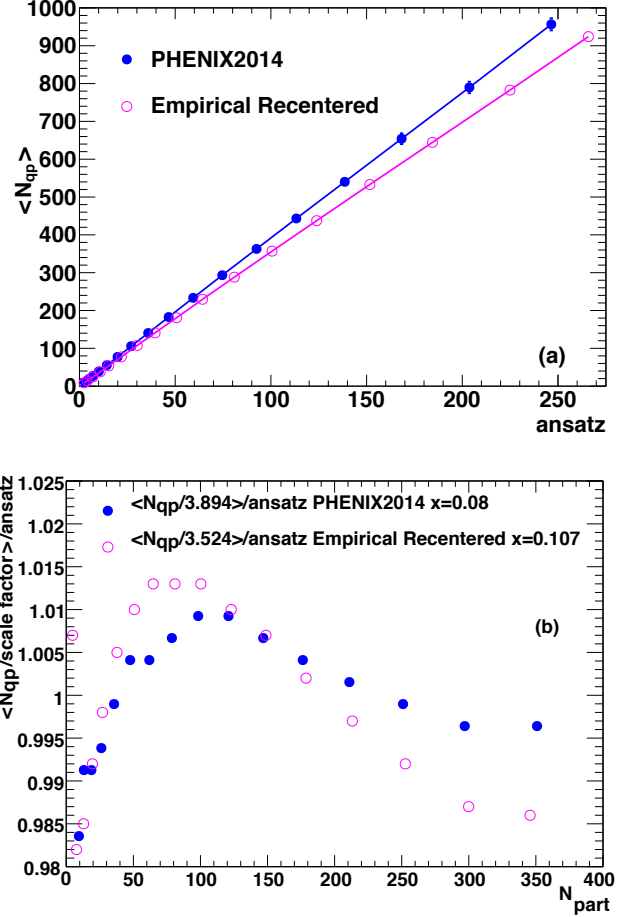
FIG. 7. a) Plot of $\langle N_{qp}\rangle$ vs. ansatz, $[(1 - x)\langle N_{part}\rangle/2 + x\langle N_{coll}\rangle]$, with $x = 0.107$, from Table VII, compared to the PHENIX2014 result [6], with $x = 0.08$ b) Plot of ratio of $(\langle Nqp\rangle/3.524)$/ansatz, where 3.524 is the average of $\langle Nqp\rangle$/ansatz for the Empirical Recentered method over the entire centrality range 0-92% in 5% bins, compared to the PHENIX2014 result [6] with average of $\langle Nqp\rangle$/ansatz =3.894

ally on top of the simplest Planar Polygon method for the Au+Au calculation rather than in agreement with the Empirical Recentered method. The Empirical Recentered method best solves the problem of maintaining the nucleon center and the correct charge distribution while keeping all the generated quark-triplets.

The agreement of the new centered methods with the Au+Au data is within 1σ for the Empirical Recentered calculation (Fig. 5b) and 1.5σ for the Planar Polygon calculation (Fig. 9b); and the new calculations agree with PHENIX2014 calculation [6] (Fig. 6) to within 1.2σ of its uncertainty for the Empirical Recentered method and 1.8σ for the Planar Polygon method. For d+Au, the NQP calculation with the Empirical Recentered method gives a result that is essentially indistinguishable from the PHENIX2014 [6] NQP result and the data (Fig. 5c).

The Empirical Recentered approach (Sec. III C) was already used in the most recent PHENIX study [26] of

$N_{\rm qp}$ scaling of midrapidity charged particle multiplicity, $dN_{\rm ch}/d\eta$, and $dE_T/d\eta$ and did show a difference of $\lesssim 2\%$ between $dN_{\rm ch}/d\eta/(0.5N_{\rm qp})$ in PHENIX2014 [6] and the Empirical Recentered value [26] as well as a similar small difference of $\langle dE_T/d\eta\rangle /N_{\rm qp} = 0.617\pm0.023$ GeV in PHENIX2014 [6] compared to the Empirical Recentered method with $\langle dE_T/d\eta\rangle /N_{\rm qp} = 0.629 \pm 0.021$ GeV [26]. Regarding the ansatz (Eq. 11), the NQP model with either the PHENIX2014 [6] or the Empirical Recentered method are consistent from $p + p$ to Au+Au collisions to within 1.5% and in fact work better than the ansatz which does not extrapolate back to the $p + p$ value [6].

It is worth pointing out that the original PHENIX2014 [6] method and the Planar Polygon method agree with the best Empirical Recentered method to within 7% lower E_T and 3% higher E_T respectively for Au+Au. These two methods have an advantage in that it is straightforward to directly apply them to any number of quarks as well as any charge distribution so that they can quickly provide a bracket around the formally correct answer. The differences between the three new methods for the Au+Au calculations can be taken as a sort of "modeling" uncertainty—one that could improve with e.g. more information about constituent-quark correlations in a nucleon.

ACKNOWLEDGMENTS

Appendix A: Full details of the NQP calculations with the new methods.

1. Original weights with no efficiency correction

The calculations of the relative probabilities w_n for $n = 2, 3, 4, 5, 6$ constituent-quark participants and σ_{q+q} in $p + p$ collisions with inelastic cross section 42 mb are given in Table I for the PHENIX2014 and the three new methods. One conclusion from Table I is that $\langle N_{\rm qp}/N_{\rm part}\rangle$ only reduces from 1.50 in PHENIX2014 to 1.35 (Planar Polygon), 1.34 (Explicit Joint) and 1.39 (Empirical Recentered), i.e. a reduction from 1.5 to 1.4. For Au+Au, the original Au+Au weights, w_n, for the PHENIX2014 [6], Planar Polygon, Explicit Joint and Empirical Recentered methods are presented in Table II.

2. Weights corrected for $p + p$ efficiency, $\epsilon_{p+p} = 1 - p_0^{p+p} = 0.647 \pm 0.065$

The method for the calculation of the E_T distribution from an $A+B$ reaction in a given detector is illustrated

TABLE I. Original weights w_n ($p_0 = 0$, $\epsilon_{p+p} \equiv 1 - p_0 = 1.0$) for $p + p$ at $\sqrt{s} = 200$ GeV for the PHENIX2014 [6] and three different new models of the positions of 3 constituent-quarks which preserve the nucleon center. Note that in Ref. [6] $\sigma = 9.36$ mb was used as the $q + q$ scattering cross section order to obtain a N+N $\sigma^{\rm inel} = 42.0$ mb. The $q + q$ scattering cross sections for the other models to obtain N+N $\sigma^{\rm inel} = 42.0$ mb are also indicated in the table as well as the $\langle N_{\rm qp}\rangle$ per $p+p$ collision ($N_{\rm part} = 2$).

$N_{\rm qp}$	PX2014 [6]	PlanarP	ExplicitJ	EmpiricalR
1	0.00000	0.00000	0.00000	0.00000
2	0.46510	0.606528	0.603101	0.54301
3	0.23789	0.179538	0.194968	0.23186
4	0.16909	0.144047	0.140203	0.14464
5	0.094588	0.050957	0.048279	0.06351
6	0.033332	0.018930	0.013449	0.01698
sum	1.0000002	1.000000	1.000000	1.000001
σ_{q+q} mb	9.36	7.72	8.15	8.17
$\langle N_{\rm qp}\rangle$	2.993	2.696	2.674	2.780

TABLE II. Original weights w_n ($p_0 = 0$, $\epsilon_{p+p} \equiv 1 - p_0 = 1.0$) for Au+Au at $\sqrt{s} = 200$ GeV for the PHENIX2014 and three different new models of the positions of 3 constituent-quarks which preserve the nucleon center.

$N_{\rm qp}$	PX2014 [6]	PlanarP	ExplicitJ	EmpiricalR
1	0.00000	0.00000	0.00000	0.00000
2	0.061275	0.050260	0.054304	0.045933
3	0.020448	0.019083	0.021482	0.021747
4	0.020923	0.024041	0.026028	0.022329
5	0.017606	0.017433	0.018562	0.018350
6	0.015731	0.016620	0.016977	0.016397
7	$\cdots$	$\cdots$		$\cdots$

for the NQP or number of quark participants model. It has been discussed in detail in Ref. [6] where it was emphasized that the key experimental issue is the linearity of the detector response to multiple collisions (better than 1% in Ref. [6]), and the stability of the response for the different $A+B$ combinations and run periods used in the analysis. The acceptance of the detector is taken into account by making a correction for the probability, p_0, of measuring zero E_T for an N+N inelastic collision, which is determined from the ratio of the measured $p + p$ cross section in the detector to the known inelastic cross section at $\sqrt{s} =200$ GeV [6] and propagated to the $q + q$ collisions, with $\epsilon_{p+p} = 1 - p_0^{p+p} = 0.647 \pm 0.065$ for the PHENIX measurement [6].

The E_T distribution is equal to the sum:

$$\left(\frac{d\sigma}{dE_T}\right)_{\rm NQP} = \sigma_{BA} \sum_{n=1}^{N_{\rm max}} w_n P_n(E_T) \qquad (A1)$$

where σ_{BA} is the measured $A+B$ cross section in the

detector, w_n is the relative probability for n quark participants in the $A+B$ reaction with minimum value $n = 2$ and maximum value $n = \text{N}_{\max}$, and $P_n(\text{E}_T)$ is the calculated E_T distribution on the detector from n independent quark participants. If $f_1(\text{E}_T)$ is the measured E_T spectrum on the detector for a quark participant that gives a nonzero E_T, and p_0 is the probability for a quark participant to produce no signal in the detector (zero E_T), then the correctly normalized E_T distribution for one quark participant is:

$$P_1(\text{E}_T) = (1 - p_0)f_1(\text{E}_T) + p_0\delta(\text{E}_T), \quad \text{(A2)}$$

where $\delta(\text{E}_T)$ is the Dirac delta function and $\int f_1(\text{E}_T)\, d\text{E}_T = 1$. $P_n(\text{E}_T)$ (including the p_0 effect) is obtained by convoluting $P_1(\text{E}_T)$ with itself $n - 1$ times

$$P_n(\text{E}_T) = \sum_{i=0}^{n} \frac{n!}{(n-i)!\, i!} p_0^{n-i} (1-p_0)^i f_i(\text{E}_T) \quad \text{(A3)}$$

where $f_0(\text{E}_T) \equiv \delta(\text{E}_T)$ and $f_i(\text{E}_T)$ is the i-th convolution of $f_1(\text{E}_T)$:

$$f_i(x) = \int_0^x dy\, f_1(y)\, f_{i-1}(x - y) \quad . \quad \text{(A4)}$$

Substituting Eq. A3 into Eq. A1 and reversing the indices gives a form that is less physically transparent, but considerably easier to compute:

$$\left(\frac{d\sigma}{d\text{E}_T} \right)_{\text{NQP}} = \sigma_{BA} \sum_{i=2}^{\text{N}_{\max}} w'_i(p_0)\, f_i(\text{E}_T) \quad \text{(A5)}$$

where

$$w'_i(p_0) = (1 - p_0)^i \sum_{n=i}^{\text{N}_{\max}} \frac{n!}{(n-i)!\, i!} p_0^{n-i}\, w_n, \quad \text{(A6)}$$

which represents the weight (or relative probability) for i convolutions of the measured $f_1(\text{E}_T)$ to contribute to the E_T spectrum in an $A+B$ collision, and where the terms with $w'_{i=0}(p_0)$ and $w'_{i=1}(p_0)$ in Eq. A5 are left out because they represent the case when no signal is observed in the detector for an $A+B$ collision since there must be at least 2 quark participants i.e.

$$w'_{i=0}(p_{0_{\text{NQP}}}) + w'_{i=1}(p_{0_{\text{NQP}}}) = p_0^{BA}. \quad \text{(A7)}$$

For a $p + p$ collision this means that Eq. A7 for $p_0^{BA} \equiv p_0^{p+p} = 1 - \epsilon_{p+p} = 0.353$ must be solved in order to find $p_{0_{\text{NQP}}}$ and $\epsilon_{\text{NQP}} = 1 - p_{0_{\text{NQP}}}$. This is done in a spreadsheet and then the corrected weights $w'_i(p_{0_{\text{NQP}}})$ for $i = 2, 3, 4, 5, 6$ quark participants are calculated for $p + p$ collisions using these $p_{0_{\text{NQP}}}$ in Eq. A6.

The results for ϵ_{NQP} for PHENIX2014 [6] and the three new methods along with the calculated corrected weights for $p + p$ collisions are presented in Table III. A test of the calculations is that the sum of the corrected weights

TABLE III. Corrected weights w'_i for $p + p$, at $\sqrt{s} = 200$ GeV. Note that $\epsilon_{p+p} = 1 - p_0^{p+p}$ is the sum of the corrected weights in the column and should equal the probability to get a non-zero E_T on a $p + p$ collision, which should and does equal 0.647.

N_{qp}	PX2014 [6]	PlanarP	ExplicitJ	EmpiricalR
	ϵ_{QP}=0.659	ϵ_{QP}=0.7074	ϵ_{QP}=0.7083	ϵ_{QP}=0.690
1	0.0000	0.00000	0.0000	0.0000
2	0.37795	0.42684	0.43082	0.41102
3	0.17296	0.14204	0.14438	0.15846
4	0.073126	0.06083	0.057330	0.060648
5	0.020168	0.01491	0.012803	0.014873
6	0.0027177	0.00237	0.0016982	0.0018326
ϵ_{p+p}	0.646922	0.64699	0.647031	0.646834

$w'_i(p_{0_{\text{NQP}}})$ for PHENIX2014 and the three new methods should equal the $p + p$ efficiency, the probability to get a non-zero E_T on a $p+p$ collision, $\epsilon_{p+p} = 1 - p_0^{p+p} = 0.647$, which works well.

The corrected weights for Au+Au are given Table IV.

TABLE IV. Corrected weights w'_i for Au+Au, at $\sqrt{s} = 200$ GeV. Note that $\epsilon_{\text{Au+Au}}$ is the sum of the corrected weights in the column and is the probability to get a non-zero E_T on an Au+Au collision.

N_{qp}	PX2014 [6]	PlanarP	ExplicitJ	EmpiricalR
	ϵ_{QP}=0.659	ϵ_{QP}=0.7074	ϵ_{QP}=0.7083	ϵ_{QP}=0.690
1	0.0000	0.0000	0.0000	0.0000
2	0.047412	0.043307	0.047077	0.041954
3	0.026998	0.027143	0.029262	0.027895
4	0.023079	0.023927	0.025123	0.023840
5	0.019473	0.019816	0.020473	0.019966
6	0.016840	0.017169	0.017710	0.017233
7	$\cdots$	$\cdots$		$\cdots$
$\epsilon_{\text{Au+Au}}$	0.956	0.968	0.966	0.968

The original (Table II) and corrected (Table IV) weights for Au+Au are plotted in Fig. 8. The weights are scaled in N_{qp} by the amounts indicated for the three new methods and all lie on top of the PHENIX2014 [6] distributions when scaled up in N_{qp} by 1.3% to 3.5% for the original weights (Fig. 8a) and scaled down in N_{qp} by 3% to 5% for the corrected weights. (Fig. 8b).

3. Calculation of the E_T distribution of a quark participant for the PHENIX2014 data [6]

The E_T distributions for $p+p$, and Au+Au at $\sqrt{s_{NN}} = 200$ GeV [6] were shown in Fig 1. They have been corrected to hadronic E_T in $\delta\phi = 2\pi$ and $\delta\eta = 1.0$. The to-
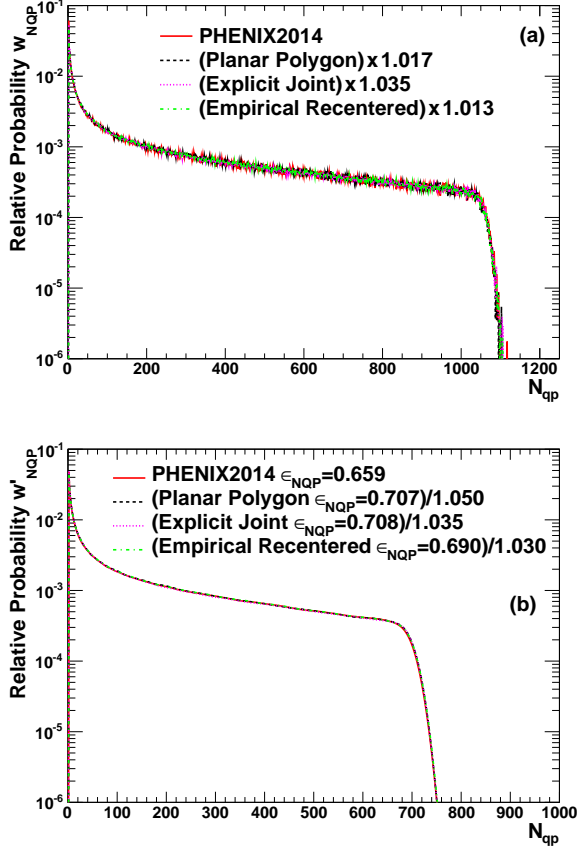
FIG. 8. Distribution of the Number of Quark Participants in Au+Au at $\sqrt{s_{NN}}$ =200 GeV scaled in N_{qp} by the indicated amounts so that they overlap the PHENIX2014 distribution [6]: a) Orignial weights w_{NQP}; b) Corrected weights w'_{NQP}.

tal number of counts in the distributions (including the counts with zero E_T which are in the lowest bin) sum up to the number of Beam Beam trigger (BBC) counts. The distributions are then normalized so that the integral is unity and represents the yield per BBC count per GeV, dY/dE_T. The lowest bin also contains counts with non-zero E_T. The E_T distribution for a $p + p$ collision is first fit to a single Gamma distribution which integrates to $Y_\Gamma^{pp} = 0.93349$ (only including the non-zero counts in the lowest bin) which is the observed yield per BBC count (see Table V). Then the BBC counts with zero in the lowest bin are removed so that only the fitted non-zero counts remain, to give the observed E_T distribution in $p + p$ which is used for all the following fits.

The E_T distribution of a quark participant is derived by assuming that the measured $p + p$ E_T spectrum in the experiment is composed of the sum of the E_T distributions emitted independently by $n = 2, 3, 4, 5, 6$ constituent-quark participants weighted by their corrected probabilities w'_n given in Table III. This is done by fitting Eq. A5 to the observed $p + p$ data, where $f_1(E_T)$

is taken as a Gamma distribution:

$$f_1(x) = \frac{b}{\Gamma(p)}(bx)^{p-1}e^{-bx}, \qquad (A8)$$

where

$$p > 0, \quad b > 0, \quad 0 \le x \le \infty \quad ,$$

$\Gamma(p)$ is is the Gamma function, which equals $(p-1)!$ if p is an integer, and $\int_0^\infty f_1(x)\,dx = 1$.

There are two reasons for this: i) in general the shape of E_T distributions in $p+p$ collisions is well represented by the Gamma distribution; and ii) the n-fold convolution (Eq. A4) is analytical i.e. $p \to np$ while b remains unchanged.

$$f_n(x) = \frac{b}{\Gamma(np)}(bx)^{np-1}e^{-bx}, \qquad (A9)$$

For this fit, which we call the deconvolution of the $p + p$ E_T distribution to its constituent-quark components (represented by Gamma distribution parameters b and p), the σ_{BA} in Eq. A5 is replaced by Y_Γ^{fit}. Also the integral of the sum of the weights times the normalized Gamma distributions which multiplies Y_Γ^{fit} is not unity but is equal to $\epsilon_{p+p} = 0.647$, so that $Y_\Gamma^{\mathrm{fit}} \times \epsilon_{p+p}$ should equal the simple integral of the $p + p$ distribution, Y_Γ^{pp}, obtained by the fit of a single Gamma distribution to the measured $p + p$ E_T distribution (Table V, NCOLL model=1 $p + p$ collision).

The derived parameters b and p of the E_T distribution of a constituent-quark for all four models are given in Table V and the $Y_\Gamma^{\mathrm{fit}} \times \epsilon_{p+p}$ agrees with the simple integral of the $p + p$ measured distribution to within 1.6% with the new models in better agreement than the original PHENIX2014 calculation.

The p+p fits and Au+Au calculations for the Planar Polygon (Sec. III A) and Explicit Joint (Sec. III B) methods are shown in Figs. 9 and 10 respectively.

TABLE V. Parameters b, p of the element indicated from the fit to $p+p$ data, cut for $E_T < 13.3$ GeV. Y_Γ^{fit} is the fitted integral of the $p+p$ distribution. For NCOLL the fit is to a single Γ distribution from which ϵ_{p+p} is calculated [6]. For the NQP models the fits are the deconvolution of elements with weights w'_i which do not sum to unity but sum to $\epsilon_{p+p} = 0.647$ so that $Y_\Gamma^{\text{fit}} \times \epsilon_{p+p}$ should equal $Y_\Gamma^{pp} = 0.93349$—the actual values are 0.948 (PHENIX2014) and 0.945 (Planar Polygon), 0.945 (Explicit Joint), 0.946 (Empirical Recentered) a good check (within 1.6%,1.3%, 1.3% and 1.3% respectively). The χ^2/dof of the deconvolution fits to the $p+p$ E_T distribution are 4907/17 (PHENIX2014) and 4841/17 (Planar Polygon), 4818/17 (Explicit Joint), 4836/17 (Empirical Recentered) which for the three centered methods are better than the single Γ fit 4866/17 (NCOLL).

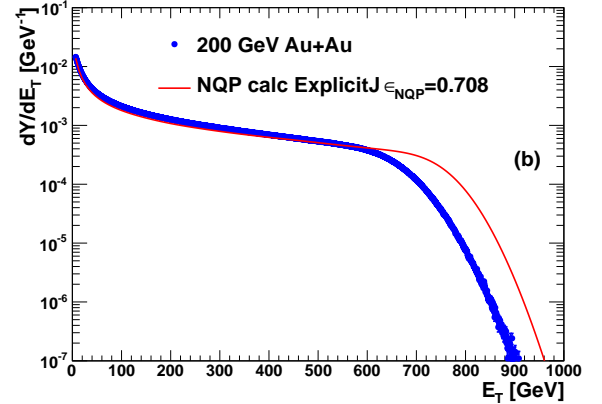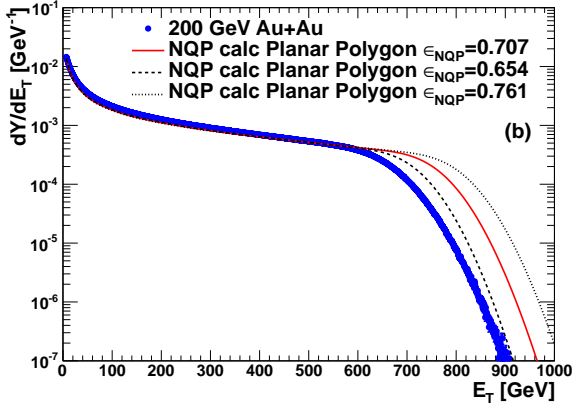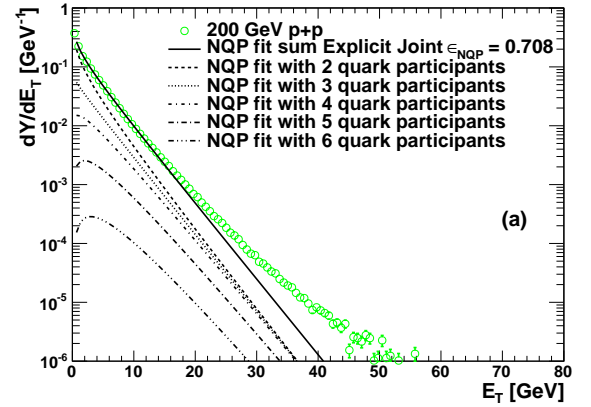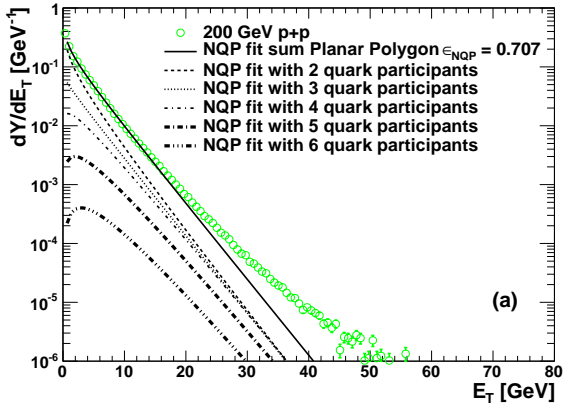| Model	$\epsilon_{\text{element}}$	element	Y_Γ^{fit}	b (GeV)$^{-1}$	p	$\langle E_T \rangle_{\text{fit}}^{\text{elem}}$ (GeV)
NCOLL	0.647	p+p	0.93349	1.8259/6.68	0.72359	0.396 ×6.68
PHENIX2014	0.659	1 QP	1.4659	1.9986/6.68	0.29740	0.1488 ×6.68
Planar Polygon	0.707	1 QP	1.4613	1.9935/6.68	0.31114	0.1561 ×6.68
Explicit Joint	0.708	1 QP	1.4605	1.9836/6.68	0.31251	0.1575 ×6.68
Empirical Recentered	0.690	1 QP	1.4626	1.9867/6.68	0.30726	0.1547 ×6.68

FIG. 9. E_T distributions at $\sqrt{s_{NN}} = 200$ GeV calculated in the Number of Quark Participants (NQP) model from the Planar Polygon method, with $\epsilon_{\text{NQP}} = 1 - p_{0_{\text{NQP}}} = 0.707$. a) NQP calculation of the $p+p$ data with the parameters p and b for the E_T distribution of 1 QP from the deconvolution fit to the same data (Table V) where the thin lines shown are the E_T distributions for 2,3,4,5 and 6 QP weighted by w'_n from Table III and the thick line is the sum. b) Au+Au calculation with systematic uncertainties.

FIG. 10. E_T distributions at $\sqrt{s_{NN}} = 200$ GeV calculated in the Number of Quark Participants (NQP) model from the Explicit Joint method, with $\epsilon_{\text{NQP}} = 1 - p_{0_{\text{NQP}}} = 0.708$. a) NQP calculation of the $p+p$ data with the parameters p and b for the E_T distribution of 1 QP from the deconvolution fit to the same data (Table V) where the thin lines shown are the E_T distributions for 2,3,4,5 and 6 QP weighted by w'_n from Table III and the thick line is the sum. b) Au+Au calculation.

TABLE VI. Uncorrected and Corrected weights, w_i and w'_i for d+Au, at $\sqrt{s} = 200$ GeV.

N_{qp}	PX2014 [6]	PX2014 [6]	EmpiricalR	EmpiricalR
	uncorrected	$\epsilon_{\mathrm{NQP}}=0.659$	uncorrected	$\epsilon_{\mathrm{NQP}}=0.690$
1	0.0000	0.0000	0.0000	0.0000
2	0.086717	0.091794	0.10191	0.10044
3	0.051578	0.072569	0.054985	0.073771
4	0.052929	0.066353	0.057050	0.066407
5	0.047335	0.060144	0.049220	0.059248
6	0.045134	0.055165	0.045505	0.054320
7	. . .	. . .	. . .	. . .

4. d+Au and AQM vs NQP

The uncorrected and corrected d+Au weights for PHENIX2014 and the Empirical recentered approach are given in Table VI. The d+Au NQP calculation with the Empirical Recentered method previously shown in Fig. 5c gives a result that is essentially indistinguishable from the PHENIX2014 [6] NQP result and the data.

5. Calculation of the ansatz

In Table VII, the centrality dependence of $\langle N_{part} \rangle$, $\langle N_{qp} \rangle$, $\langle N_{\mathrm{coll}} \rangle$ is presented, together with the ansatz calculated for $x = 0.107$ in the Empirical recentered approach, which gives the best result. The average of the $\langle N_{\mathrm{qp}} \rangle /$ansatz $= 3.524$ over the entire centrality range in Au=Au from 0-92% in 5% bins and varies within $\pm 1.5\%$ over this range, still an excellent result. Figure 7 showed the linearity of N_{qp} vs. the ansatz compared to the PHENIX2014 [6] result, with the best values of x in each case (top); and the $\lesssim 1.5\%$ deviations of $\langle N_{\mathrm{qp}} \rangle /$ansatz$/\langle\langle N_{\mathrm{qp}} \rangle /$ansatz$\rangle$ from 1.00 on an expanded scale (bottom).

The fact that the $\langle N_{\mathrm{qp}} \rangle /$ansatz ratio drops from an average of 3.524 for Au+Au collisions to 2.78 for $p+p$ collisions is also interesting. This is consistent with the PHOBOS [29] result that a fit of Eq. 11 to $\langle dN_{\mathrm{ch}}{}^{AA}/d\eta \rangle$ with $x = 0.09$ leaving $\langle dN_{\mathrm{ch}}{}^{pp}/d\eta \rangle$ as a free parameter gives the result $\langle dN_{\mathrm{ch}}{}^{pp}/d\eta \rangle = 2.70$ which is above the measured inelastic value of 2.29. The lower value of $\langle N_{\mathrm{qp}} \rangle /$ansatz for $p+p$ would then give a value of $2.70 \times 2.78/3.524 = 2.13$ for $\langle dN_{\mathrm{ch}}{}^{pp}/d\eta \rangle$, much closer to the measured value. This shows that the N_{qp} model is consistent from from $p+p$ to Au+Au collisions and so actually works better than the ansatz.

TABLE VII. Test of whether the ansatz, $[(1-x)\langle N_{\text{part}}\rangle/2 + x\langle N_{\text{coll}}\rangle]$, from Eq. 11, with $x = 0.107$, is a proxy for $\langle N_{\text{qp}}\rangle$. The errors are not quoted on $\langle N_{part}\rangle$, $\langle N_{qp}\rangle$, $\langle N_{\text{coll}}\rangle$ because they are correlated Type C and largely cancel for the $\langle N_{\text{qp}}\rangle$/ansatz ratio.

Centrality	$\langle N_{part}\rangle$	$\langle N_{qp}\rangle$	$\langle N_{\text{coll}}\rangle$	ansatz	$\langle N_{\text{qp}}\rangle$/ansatz	$\langle N_{\text{qp}}\rangle$/ansatz/$\langle\langle N_{\text{qp}}\rangle$/ansatz$\rangle$
0-5%	345.7	924.2	1042.5	265.9	3.476	0.986
5-10%	299.9	782.6	850.3	224.9	3.480	0.987
10-15%	252.7	644.5	668.7	184.4	3.496	0.992
15-20%	213.2	533.1	527.7	151.7	3.515	0.997
20-25%	178.7	437.5	412.1	123.9	3.531	1.002
25-30%	148.8	356.9	318.8	100.6	3.549	1.007
30-35%	122.9	288.2	243.4	80.9	3.561	1.010
35-40%	100.3	229.6	182.7	64.3	3.570	1.013
40-45%	81.0	180.9	135.4	50.7	3.572	1.013
45-50%	64.8	141.0	98.9	39.5	3.570	1.013
50-55%	50.8	107.7	70.6	30.2	3.561	1.010
55-60%	37.8	77.5	47.0	21.9	3.542	1.005
60-65%	27.0	53.7	29.9	15.3	3.517	0.998
65-70%	19.5	37.7	19.5	10.8	3.497	0.992
70-75%	12.9	24.3	11.6	7.0	3.473	0.985
75-80%	7.6	14.0	6.1	4.0	3.460	0.982
80-92%	4.7	8.6	3.3	2.4	3.549	1.007
$p+p$	2	2.78	1	1	2.78	0.79

[1] Michael L. Miller, Klaus Reygers, Stephen J. Sanders, and Peter Steinberg, "Glauber modeling in high energy nuclear collisions," Ann.Rev.Nucl.Part.Sci., **57**, 205–243 (2007).

[2] R. Hofstadter, "Electron scattering and nuclear structure," Rev. Mod. Phys., **28**, 214 (1956).

[3] M. Gell-Mann, "A schematic model of baryons and mesons," Phys. Lett., **8**, 214–215 (1964).

[4] A. H. Mueller, "QCD at high energies," Nucl. Phys. A, **527**, 137c–152c (1991).

[5] G. Dillon and G. Morpurgo, "The general qcd parametrization and the hierarchy of its parameters: Why some simple models of hadrons work so well," Revista del Nuovo Cimento, **33**, 1–55 (2010).

[6] S. S. Adler *et al.* (PHENIX Collaboration), "Transverse-energy distributions at midrapidity in $p + p$ d+Au and Au+Au collisions at $\sqrt{s_{NN}} = 62.4 - 200$ GeV and implications for particle-production models," Phys. Rev. C, **89**, 044905 (2014).

[7] S. S. Adler *et al.* (PHENIX Collaboration), "Systematic studies of the centrality and $\sqrt{s_{NN}}$ dependence of the $dE_T/d\eta$ and $dN_{ch}/d\eta$ in heavy ion collisions at midrapidity," Phys. Rev. C, **71**, 034908 (2005).

[8] A. Białas, M. Bleszyński, and W. Czyż, "Multiplicity distributions in nucleus-nucleus collisions at high energies," Nucl. Phys. B, **111**, 461–476 (1976).

[9] J Ftacnik, K. Kajantie, N. Pisutova, and J. Pisut, "On the transverse energy distributions in the central rapidity region of ^{16}O+Pb collisions at 200 GeV per nucleon," Phys. Lett. B, **188**, 279–282 (1987).

[10] T. Abbott *et al.*, "Measurement of energy emission from O+A and p+A collisions at 14.5 GeV/c per nucleon with a lead-glass array," Phys. Lett. B, **197**, 285–290 (1987).

[11] T. Abbott *et al.*, "Systematics of midrapidity transverse energy distributions in limited apertures from p+Be to Au+Au collisions at relativistic energies," Phys. Rev. C, **63**, 064602 (2001).

[12] A. Bialas, W. Czyz, and L. Lesniak, "Additive quark model of multiparticle production and nucleus-nucleus collisions at high energies," Phys. Rev. D, **25**, 2328–2340 (1982).

[13] A. Bialas and A. Bzdak, "Wounded quarks and diquarks in heavy ion collisions," Phys. Lett. B, **649**, 263–268 (2007).

[14] B. Alver *et al.*, "Charged-particle multiplicity and pseudorapidity distributions measured with the PHOBOS detector in Au + Au, Cu + Cu, d + Au, and p + p collisions at ultrarelativistic energies," Phys. Rev. C, **83**, 024913 (2011).

[15] K. Adcox *et al.* (PHENIX Collaboration), "Centrality dependence of charged particle multiplicity in Au+Au collisions at $\sqrt{s_{NN}} = 130$ GeV," Phys. Rev. Lett., **86**, 3500–3505 (2001).

[16] K. Adcox *et al.* (PHENIX Collaboration), "Measurement of the midrapidity transverse energy distribution from $\sqrt{s_{NN}} = 130$ GeV Au+Au collisions at RHIC," Phys. Rev. Lett., **87**, 052301 (2001).

[17] S. Eremin and S. Voloshin, "Nucleon participants or quark participants?" Phys. Rev. C, **67**, 064905 (2003).

[18] R. Nouicer, "Charged particle multiplicities in A + A and p + p collisions in the constituent quarks framework," Eur. Phys. J. C, **49**, 281–286 (2007).

[19] B. De and S. Bhattacharyya, "Rapidity spectra of the secondaries produced in heavy ion collisions and the constituent picture of the particles," Phys. Rev. C, **71**, 024903 (2005).

[20] A. Bialas, "Wounded nucleons, wounded quarks: an update," J. Phys., **G 35**, 044053 (2008).

[21] C. De Marzo *et al.*, "A study of high transverse energy interactions of 150 and 300 GeV pions and protons on a hydrogen target using a large acceptance calorimeter," Nucl. Phys. B, **211**, 375–413 (1983).

[22] J. A. Appel *et al.*, "Experimental study of the emergence of two-jet dominance in $\bar{\text{p}}$+p collisions at $\sqrt{s} = 630$ GeV," Phys. Lett. B, **165**, 441–448 (1985).

[23] R. Hofstadter, F. Bumiller, and M. R. Yerian, "Electromagnetic structure of the proton and neutron," Rev. Mod. Phys., **30**, 482 (1958).

[24] L. N. Hand, D. G. Miller, and R. Wilson, "Electric and Magnetic Form Factors of the Nucleon," Rev. Mod. Phys., **35**, 335 (1963).

[25] J. C. Bernauer *et al.* (A1 Collaboration), "Electric and magnetic form factors of the proton," Phys. Rev. C, **90**, 015206 (2014).

[26] A. Adare *et al.* (PHENIX Collaboration), "Transverse energy production and charged-particle multiplicity at midrapidity in various systems from $\sqrt{s_{NN}} = 7.7$ to 200 GeV," Phys. Rev. C, **93**, 024901 (2016).

[27] A. Adare *et al.* (PHENIX Collaboration), "Identified charged hadron production in $p+p$ collisions at $\sqrt{s} = 200$ and 62.4 GeV," Phys. Rev. C, **83**, 064903 (2011).

[28] X.-N. Wang and M. Gyulassy, "Energy and centrality dependence of rapidity densities at RHIC energies," Phys. Rev. Lett., **86**, 3496–3499 (2001).

[29] B. Back *et al.*, "Collision geometry scaling of Au+Au pseudorapidity density from $\sqrt{s_{NN}} = 19.6$ to 200 GeV," Phys. Rev. C, **70**, 021902(R) (2004).

[30] L. Zhou and G. S. F. Stephans, "Energy and centrality dependence of particle multiplicity in heavy ion collisions from $\sqrt{s_{NN}} = 20$ to 2760 GeV," Phys. Rev. C, **90**, 014902 (2014).